J Nanostruct 7(4): 292-308, Autumn 2017

RESEARCH PAPER

Enhanced Electrocatalytic Activity of Pt-M (M= Co, Fe) Chitosan Supported Catalysts for Ethanol Electrooxidation in Fuel Cells

Mehri-Saddat Ekrami-Kakhki [1] , Jilla Saffari [2], Nahid Farzaneh [1] and Sedigheh Abbasi [1]*

[1] *Nano Technology Laboratory, Engineering Department, Esfarayen University of Technology, Esfarayen, Iran*

[2] *Young Researchers and elite club, Zahedan Branch, Islamic Azad University, Zahedan, Iran*

ARTICLE INFO

Article History:
Received 03 August 2017
Accepted 12 September 2017
Published 01 October 2017

Keywords:
Bimetallic
Chitosan
Ethanol Electrooxidation
Fuel Cell
Nanoparticles

ABSTRACT

Here, metal nanoparticles were synthesized by chemical reduction of the corresponding metal salts in the presence of chitosan polymer. Binary and ternary metallic-chitosan Pt-Fe-CH, Pt-Co-CH and Pt-Fe-Co-CH nanocomposites were prepared. Transmission electron microscopy images and UV–Vis spectra of the nanocomposites confirmed the presence of the metal nanoparticles. The electrocatalytic activity of the nanocomposites for ethanol oxidation was tested by cyclic voltammetry, Liner Sweep Voltammetry, amperometric i-t curve and electrochemical impedance spectroscopy techniques. The effect of some experimental factors on ethanol oxidation was investigated. CO stripping was used to determine the CO tolerance of the catalysts for ethanol oxidation. Incorporation of small amounts of Co and Fe nanoparticles in the Pt-CH catalyst caused the higher activity of the catalyst for ethanol electrooxidation. The activation energy of Pt-Co-Fe-CH catalyst obtained from the Arrhenius equation was lower than other studied catalysts. These results showed that Pt-Fe-Co-CH catalyst has better catalytic activity for ethanol oxidation among all prepared catalysts.

How to cite this article
Ekrami-Kakhki M. S , Saffari J, Farzaneh N, Abbasi S. Enhanced Electrocatalytic Activity of Pt-M (M= Co, Fe) Chitosan Supported Catalysts for Ethanol Electrooxidation in Fuel Cells. J Nanostruct, 2017; 7(4):292-308.

INTRODUCTION

In recent years, much attention has been paid to a direct alcohol fuel cell (DAFC), because a direct-fed liquid fuel cell is ideal for portable applications due to its compact system and high energy density fuel storage [1-3]. However, the real commercialization of DAFCs is still hindered by significant energy loss. The major losses are caused by the poor activity of the oxidation of methanol as the simplest alcohol and its crossover from the anode to the cathode that leads a decreased cathode potential [4]. So to develop an appropriate fuel for a DAFC, some organic fuels such as oxidation of ethanol [5], dimethoxymethane [6], formic acid [7], propane [8] and ethylene glycol [9] have been studied. However, these fuels still have some problems regarding their electrochemical activity, energy density and crossover problem. Oxidation of ethanol is more difficult than that of methanol with the necessity of breaking the C–C bond for complete oxidation. Increasing the electroactivity of ethanol and its complete oxidation is a crucial task and is a hard challenge [10]. It is reported that ethanol is oxidized to acetaldehyde and CO_2 by a dual-path mechanism in which the oxidation to acetaldehyde and CO_2 was occurred by the dehydrogenation of adsorbed ethanol and adsorbed intermediates, respectively [11]. The complexity of this reaction and the presence of so many intermediates require the development of novel anode catalysts, able to break the C–C bond, to release 12 electrons and to completely oxidize the poisoning species at lower over potentials [12]. CO can be easily removed by incorporating

* *Corresponding Author Email: ekrami@esfarayen.ac.ir*

of transition metal into the Pt catalyst, but this improvement requires cost and stability. In order to design new catalysts, the properties of Pt and Pt-containing systems needs to be superior understood [13]. Recent research on the oxidation of ethanol is centered on the development of appropriated catalysts. PtMnCuX (X= Fe, Co, Ni and Sn) and PtMnMoX/C (X= Fe, Co, Ni, Cu and Sn) have been studied as suitable materials [14]. Several polymers are very convenient supports for dispersing catalytic materials at the molecular level in such a way that each catalytic center will be accessible to the reactive molecules. Chitosan (CH) offers great advantages due to its non-toxicity and suitable adhesion to the electrode substrate [15]. The addition of chitosan into noble metal containing catalysts can significantly improve the electrode performance for alcohol oxidation.

In the present work, a very simple method was used for preparation of Pt and Pt-based catalysts in the presence of chitosan as the support. Initially, we investigated the catalytic oxidation of ethanol on platinum nanoparticles (NPs) dispersed into chitosan (PtNPs-CH). In order to improve the catalytic activity of Pt, we prepared binary and ternary catalysts dispersed in chitosan, PtNPs-M-CH (M=Co, Fe) and PtNPs-CoNPs-FeNPs-CH for electrooxidation of ethanol. To prepare nanocomposites, suitable metal ions were reduced into zero valent nanoparticles in the chitosan solution. The prepared nanoparticles were characterized by UV-Vis spectra and transmission electron microscopy (TEM). The electrochemical activity of PtNPs-CH, PtNPs-M-CH (M = Co, Fe) and PtNPs-CoNPs-FeNPs-CH nanocomposites toward ethanol oxidation (EO) reaction were investigated by cyclic voltammetry (CV), Liner Sweep Voltammetry (LSV) and amperometric i-t curve measurement (i-t) techniques. Comparative studies of the electrocatalytic activity of the nanocomposites were carried out toward ethanol oxidation reaction (EOR). Different parameters affecting on EO at the prepared catalysts were investigated. The influence of temperature on the electrochemical properties of the nanocomposites was also investigated and the activation energies of EOR were calculated using the Arrhenius equation.

MATERIAL AND METHODS

Preparation of the nanocatalysts

PtNPs-CH, PtNPs-FeNPs-CH, PtNPs-CoNPs-CH and PtNPs-CoNPs-FeNPs-CH catalysts were prepared by chemical reduction of the proper metal precursors, H_2PtCl_6 (Merck), $CoCl_2.6H_2O$ (Merck) and $FeCl_3.6H_2O$ (for analysis, Merck) with $NaBH_4$ (Merck) as the reducing agent. At first, a solution of chitosan ([2-amino-2-deoxy-(1-4)-β-D-glucopyranose], with medium molecular weight, 400000 Da, Fluka) (2 mg/ml) was prepared in 1% acetic acid (glacial, Merck) solution. Due to the poor solubility of chitosan, the mixture was stirred to completely dissolve and kept for overnight. The solution was filtrated through 0.22 m Millipore syringe filters to remove any impurity before use. To ensure the entire reduction, the concentration of $NaBH_4$ was 10 times that of metal salt. In a typical procedure, a 25 µl metal salts ($CoCl_2.6H_2O$ (0.04 M), $FeCl_3.6H_2O$ (0.04 M) and H_2PtCl_6 (1M) or a mixture of metal salts aqueous solution) was mixed with 3 ml of chitosan solution, the mixtures were stirred using a rotary aperture (100 rpm) for 90 min, then freshly prepared aqueous solutions of $NaBH_4$ (50µl, 0.4M) were added to the mixture, and stirred for another 30 min until the entire reduction of metal salts. Metal–chitosan nanocomposites were formed by adsorbing of metal nanoparticles onto the surface of chitosan molecules.

The prepared nanocomposites were kept at room temperature for characterization. The doubly distilled water was used for preparation of the aqueous solutions.

Characterization

The size, shape and dispersion of the nanoparticles were determined by TEM images. TEM images were taken with using a Philips CM120 transmission electron microscope with the resolution ~ 2.5 Å. An analytikjena SPE-CORD S100 spectrometer with photodiode array detector recorded UV-Vis spectra of the nanocomposites.

Electrochemical investigations

The electrochemical characterizations of the PtNPs-CH, PtNPs-FeNPs-CH, PtNPs-CoNPs-CH and PtNPs-FeNPs-CoNPs-CH catalysts were carried out with a potentiostat/galvanostat Autolab (Nova software model PGSTAT 302N, Metrohm, Netherlands) controlled by a personal computer in a conventional three-electrode cell. A saturated calomel electrode (SCE) was used as the reference electrode and a platinum electrode served as the counter electrode. The glassy carbon (GC)

electrode with 2 mm of diameter polished with 0.05 µm alumina slurry and coated with a thin layer of the nanocomposites was served as the working electrode.

Before coating the catalyst layer, the polished GC electrode was sonicated in water and absolute ethanol, cleaned and activated by cyclic voltammetry technique between −1.5 and +1.5 V in freshly prepared deoxygenated 1.0 mol.L^{-1} H_2SO_4. 5 µL of the nanocomposites was deposited onto an activated GC electrode, and then was dried under IR radiation for 10 min. The electrolyte solutions, made of 30 ml of 0.5 M H_2SO_4 or 0.5 M H_2SO_4 and 1.07 M C_2H_5OH, were purged with N_2 for 30 min prior to each measurement. All the electrochemical investigations were done at the scan rate of 100 mV s^{-1}.

RESULTS AND DISCUSSION

Spectroscopic and microscopic analysis

Formation of the nanoparticles was confirmed by UV–Vis spectra and TEM observations. The UV–Vis spectrum of platinum chitosan nanocomposite was shown in Fig. 1A. As seen, the absorption peak of Pt (IV) species spectrum which observed at ~ 265 nm (Fig. 1A (a)) [16], disappeared completely after the reaction. This indicated that Pt (IV) species used up and the colloidal Pt nanoparticles formed (Fig. 1A (b)). UV-Vis spectra of cobalt and iron chitosan nanocomposites were shown in Fig. 1B. UV-Vis spectrum of $CoCl_2$ solution was indicated in Fig. 1B (a). It is clear that there is not any absorption peak for $CoCl_2$ solution in the range of 230 - 890 nm. Fig. 1B (b) showed the UV-Vis absorption spectrum of Co nanoparticles dispersed in chitosan. The absorption peak of the spectrum at 300 nm was attributed to the formation of Co nanoparticles [17]. Formation of iron nanoparticles was also detected by UV-Vis spectrum (see Fig. 1B (c)). Absorptions peaks of the spectrum were seen at two wavelengths (230 and 340 nm). The observed shifts in peaks of the nanoparticles may be due to media compositions or particles size [18]. UV-Vis spectrum of $FeCl_2$ solution has been shown in Fig. 1B (d). TEM image of Pt nanoparticles and their distribution in chitosan was shown in Fig. 1C.

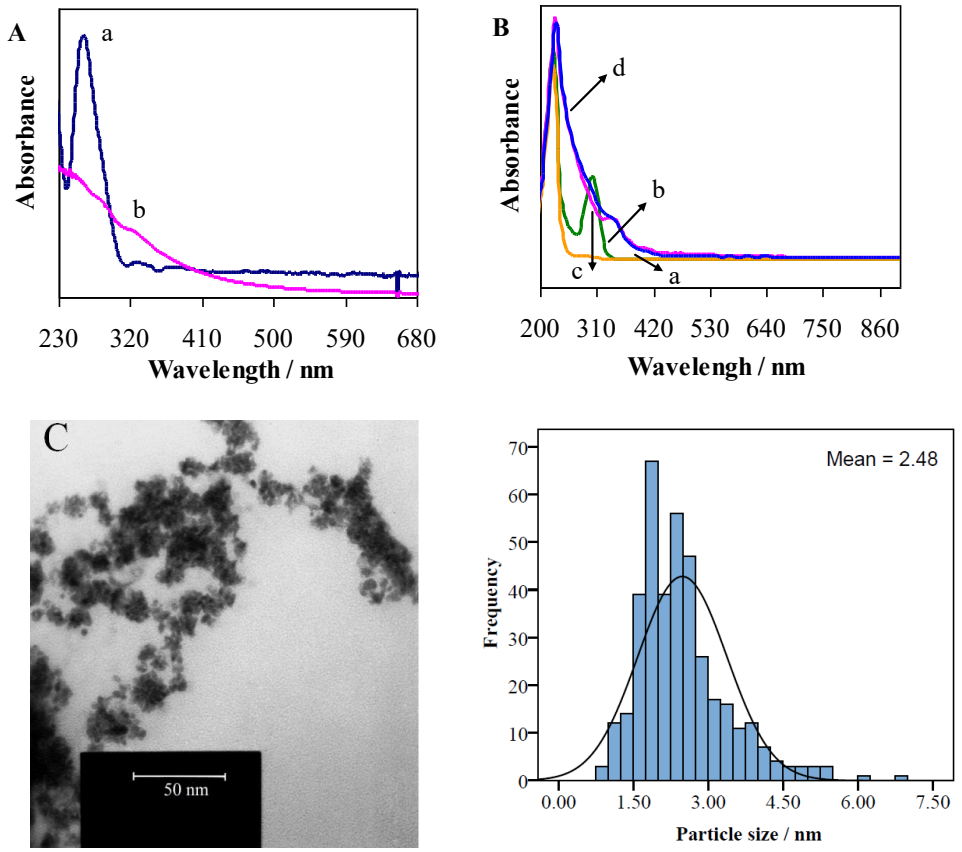

Fig. 1. UV–Vis absorption spectra of A(a) H_2PtCl_6 solution, A(b) Pt nanoparticles, B(a) $CoCl_2$ solution, B(b) Co nanoparticles, B(c) Fe nanoparticles, B(d) $FeCl_2$ solution dispersed in chitosan, C TEM image of Pt nanoparticles and their distribution in chitosan.

As seen, Pt nanoparticles were spherical and nano-size. The overall size of Pt nanoparticles ranged around 1 to 4 nm with the mean size of 2.48 nm. Fig. 2 showed TEM images of PtNPs-CoNPs, PtNPs-FeNPs and PtNPs-CoNPs-FeNPs dispersed in chitosan.

TEM image of PtNPs-FeNPs-CH was shown in Fig. 2a. As seen, there was a good dispersion of Pt and Fe nanoparticles in chitosan solution. Fig. 2a clearly indicated that the prepared Pt and Fe nanoparticles were spherical and ranged around 2 to 4.5nm with the mean size of 3.02 nm. Fig. 2b showed TEM image of PtNPs-CoNPs dispersed in chitosan. As seen, Pt and Co nanoparticles were successfully synthesized. They were spherical and there was a very good dispersion of the prepared nanoparticles in chitosan. The overall size of the nanoparticles ranged around 1 to 4 nm with the mean size of 2.37 nm.

TEM image of PtNPs-CoNPs-FeNPs dispersed in chitosan has been shown in Fig. 2c. As seen, nanoparticles were spherical and ranged around

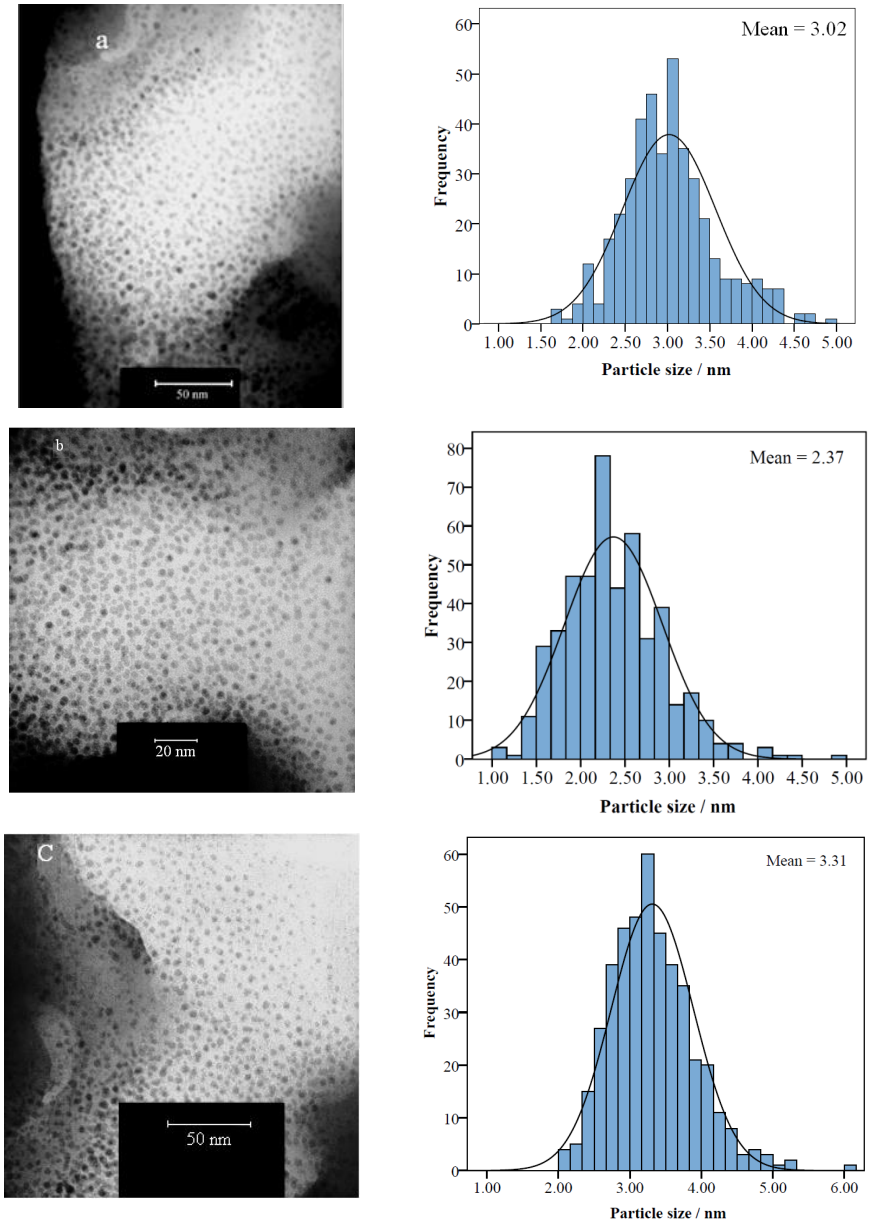

Fig. 2. TEM images of (a) platinum-iron, (b) platinum-cobalt and (c) platinum-cobalt-iron nanoparticles distributed in chitosan.

2 to 5 nm with the mean size of 3.31 nm. There was a very good dispersion of the nanoparticles in chitosan. This was due to the chitosan usage which allows a better dispersion of nanoparticles via larger portion of the surface and thus prevents the agglomeration of the metallic particles.

Electrochemical characterization

The electrochemically active surface area (EASA) of PtNPs is a main parameter for investigation of the catalytic activity, especially for an oxidation reaction as a surface and heterogeneous reaction. EASA can be calculated through the CV technique with the voltammograms of H_2 adsorption/desorption of the modified electrodes (Fig. 3). The platinum EASA of the modified electrodes can be calculated with determination of the columbic charge (Q_H) for hydrogen adsorption/desorption. Q_H is the mean value between the amounts of charge exchanged during the electrochemically adsorption (Q''_H) and desorption (Q'_H) of H_2 molecules on the Pt sites [19] (Eq. 1).

$$Q_H = (Q'_H+Q''_H)/2 \quad (1)$$

It was calculated by determining the area under the peak at the potential rang of hydrogen adsorption/desorption on the prepared electrodes.

The EASA amount for Pt nanoparticles was calculated with Q_H and Eq. (2) [20-22]:

$$EAS=Q_H/S\times L \quad (2)$$

S is a factor relating the charge to area (= 0.21 $mC.m^{-2}$). This factor indicates the charge required for oxidation of a H_2 adsorbed monolayer on the Pt particles. L is the Pt loading ($mg.cm^{-2}$) that was ~ 0.51$mg.cm^{-2}$ for the modified electrodes. The calculated EASA amounts of PtNPs-CH, PtNPs-FeNPs-CH, PtNPs-CoNPs-CH and PtNPs-CoNPs-FeNPs-CH catalysts with similar Pt loading were 39.78, 50.59, 68.24 and 148.44, respectively. As observed, PtNPs-CoNPs-FeNPs-CH nanocatalyst had the highest EASA value among other prepared catalysts showing that this nanocatalyst had the highest catalytic activity for EO reaction. As seen, EASA amount of as-prepared nanocatalysts were as follows:

PtNPs-CH<PtNPs-FeNPs-CH<PtNPs-CoNPs-CH<PtNPs-CoNPs-FeNPs-CH

CO stripping voltammograms were investigated to get more information about the CO oxidation characteristics on the catalysts. Fig. 4A (a-d) showed the adsorbed CO (CO_{ads}) stripping voltammograms for the PtNPs-CH (Fig. 4Aa), PtNPs-FeNPs-CH (Fig. 4Ab), PtNPs-CoNPs-CH (Fig. 4Ac) and PtNPs-CoNPs-FeNPs-CH (Fig. 4Ad) catalysts in 0.5M H_2SO_4. CO was purged while holding the potential at 0.20 V vs. SCE for CO

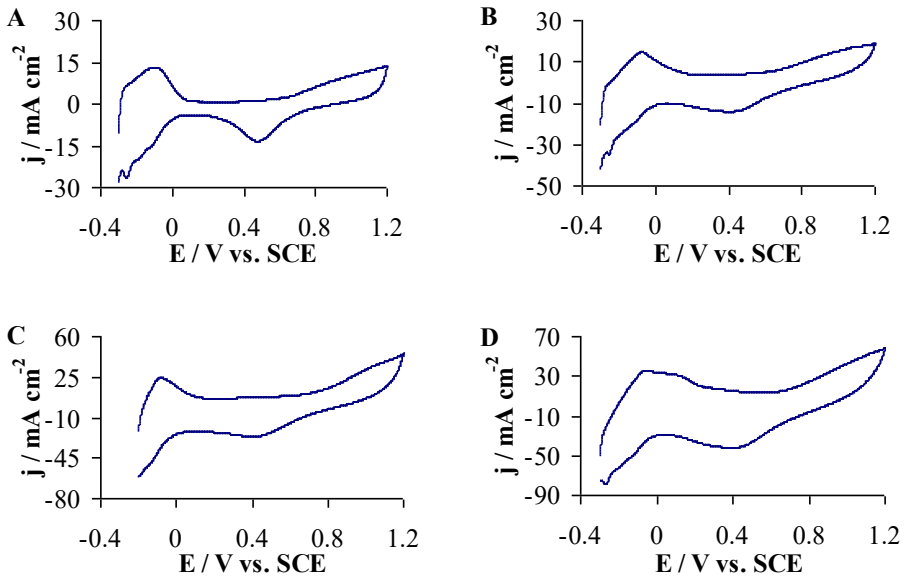

Fig. 3. CV curves of A) PtNPs-CH, B) PtNPs-FeNPs-CH, C) PtNPs-CoNPs-CH and D) PtNPs-CoNPs-FeNPs-CH catalysts in 0.5 M H_2SO_4.

adsorption. The adsorption time of CO was set to 20 min. Further increase in the adsorption time did not have any effect on the voltammograms. All stripping voltammograms showed a single CO oxidation peak. To remove the dissolved CO, the solution was purged with N_2 for 30 min before the stripping test. No CO oxidation was determined in the second scan indicating the complete removal of the CO_{ads} species. For the PtNPs-CH catalyst, a sharp CO oxidation peak appeared at 0.7V and the onset potential of CO oxidation was 0.62 V (Fig. 4Aa). As seen in fig. 4Ab, for PtNPs-FeNPs-CH catalyst, the CO oxidation peak appeared at 0.64 V and the onset potential was 0.54 V. For the PtNPs-CoNPs-CH catalyst, a sharp CO oxidation peak appeared at 0.68V and the onset potential of CO oxidation was 0.60 V (Fig. 4Ac). As observed in Fig. 4Ad, for PtNPs-CoNPs-FeNPs-CH catalyst, the CO oxidation peak appeared at 0.59 V and the onset potential of CO oxidation was 0.36 V. The potential of CO oxidation peak and also the onset potential of CO oxidation peak for all as-prepared catalysts were as follows:

PtNPs-CoNPs-FeNPs-CH<PtNPs-FeNPs-CH<PtNPs-CoNPs-CH<PtNPs-CH

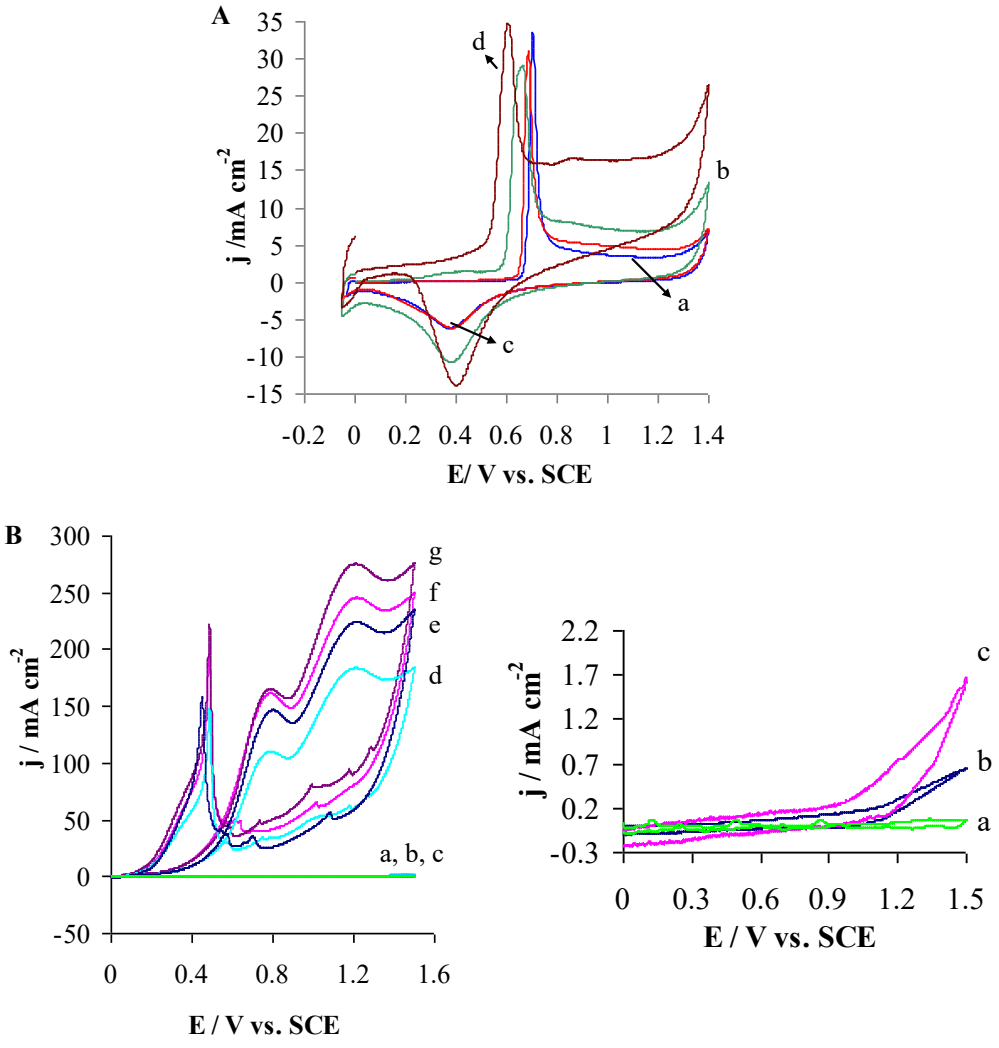

Fig. 4. A) CO stripping voltammograms of a) PtNPs-CH, b) PtNPs-FeNPs-CH, c) PtNPs-CoNPs-CH, d) PtNPs-CoNPs-FeNPs-CH catalysts in 0.5M H2SO4. B) Cyclic voltammograms for EO in 1.07 M ethanol and 0.5 M H_2SO_4 at a) GC/CH, b) GC/CoNPs-CH, c) GC/FeNPs-CH, d) GC/PtNPs-CH, e) GC/PtNPs-FeNPs electrodes, f) GC/PtNPs-CoNPs-CH and g) GC/PtNPs-CoNPs-FeNPs-CH electrodes. (CV at GC electrode is not shown, which is similar to that of GC/CH electrode) (Fig. 4B (a), (b), and (c) are shown in the inset).

The negative shift in the peak potential and onset potential of CO oxidation peak might show faster charge transfer kinetics of the CO oxidation process [23]. The oxidation peak of CO_{ads} for PtNPs-CoNPs-FeNPs-CH catalyst was more negative than PtNPs-FeNPs-CH, PtNPs-CoNPs-CH and PtNPs-CH catalysts. This shows that CO_{ads} oxidation is energetically more favorable at PtNPs-CoNPs-FeNPs-CH catalyst. The lower peak potential for CO oxidation at PtNPs-CoNPs-FeNPs-CH catalyst is probably due to the presence of the oxygenated species on Co and Fe sites at lower potentials compared to platinum [24–26].

Ethanol oxidation reaction (EOR)

Electrochemical properties of the modified electrodes have been investigated by cyclic voltammetry in 1.07 M C_2H_5OH and 0.5 M H_2SO_4 aqueous solution and the typical cyclic voltammograms for GC/CH, GC/CoNPs-CH, GC/FeNPs-CH, GC/PtNPs-CH, GC/PtNPs-CoNPs-CH, GC/PtNPs-FeNPs-CH and GC/PtNPs-CoNPs-FeNPs-CH nanocomposites were shown in Fig. 4B. No current peaks of EO can be observed in the CV curves of the GC and GC/CH electrodes (Fig. 4B (a)), which indicates that the GC and GC/CH substrate has no obvious electrocatalytic activity for EO (CV at GC electrode was not shown, which was similar to that of GC/CH electrode). Cyclic voltammograms of GC/CoNPs-CH and GC/FeNPs-CH electrodes were shown in Fig. 4B (b) and 4B (c). As can be seen these electrodes has no obvious electrocatalytic activity for EO. Fig. 4B (a), 4B (b) and 4B (c) were shown obviously in the inset of Fig. 4B. On the other hand, the typical cyclic voltammogram for ethanol electrooxidation in 0.5 M H_2SO_4 obtained with a GC/CH electrode containing the PtNPs dispersed electrocatalyst (GC/PtNPs-CH) was presented in the Fig. 4B (d) and high electrocatalytical activity was observed. The electrocatalytic activity of the electrode depends on the portion of the surface which available to participate in the dispersion of metallic particles. It has been reported that the use of a more porous matrix of conductive polymers allows a better dispersion of electrocatalytic particles through larger portion of the surface and thus prevent agglomeration of metallic particles [27]. As seen in Fig. 4B (d), two oxidation peaks for EO can be observed during the forward scan at 0.785 (J_{f1}) and 1.203 V (J_{f2}). The third oxidation peak of ethanol electrooxidation on the GC/PtNPs-CH electrode was seen during the backward scan at 0.486 V.

As mentioned in the literature [28, 29], three oxidation peaks can be seen for ethanol electrooxidation. Two oxidation peaks can be observed during the forward scan. The first oxidation current peak (J_{f1}) mainly occurred due to the CO_2 formation. After the first peak, the current density decreased slightly. This happened due to the oxidation of the Pt nanoparticles on the surface which decreased the number of active sites. In the following, with increasing the potential, the current density increased again and the second oxidation peak (J_{f2}) appeared. In fact, the EO reaction could occur on the Pt oxide surface at such a high potential. Formation of CH_3CHO caused formation of the second oxidation peak (peak J_{f2}) [28]. In the backward potential sweep, Pt oxide is reduced to platinum and produced clean PtNPs surface. In these surface, ethanol electrooxidation occurs and the current peak (J_b) observes.

In order to investigate the effect of CoNPs and FeNPs on the electrocatalytic activity of GC/PtNPs-CH electrode, the content of Pt was kept at a constant value (8 mM) and the concentration of metal nanoparticles was 0.33 mM. Fig. 4B (e) displayed the representative CV of ethanol electrooxidation obtained on GC/PtNPs-FeNPs-chitosan electrode. As seen in Fig. 4B (e), high electrocatalytic activity was observed. The electrocatalytic activity of PtNPs-FeNPs-CH toward ethanol electrooxidation was higher than that of PtNPs-CH catalyst. Two oxidation peaks for the EO reaction can be observed during the forward scan at 0.793 and 1.215 V. The third oxidation peak of EO on GC/PtNPs-FeNPs-chitosan electrode was seen during the backward scan at 0.449 V. Fig. 4B (f) showed the electrooxidation of ethanol on GC/PtNPs-CoNPs-chitosan electrode. As Seen, two oxidation peaks of ethanol electrooxidation can be seen during the forward scan at 0.787 V (J_{f1}) and 1.213 V (J_{f2}), respectively. The third oxidation peak was observed during the backward scan at 0.485 V (J_b). Electrooxidation of ethanol on GC/PtNPs-CoNPs-FeNPs was shown at Fig. 4B (g). As observed, two oxidation peaks were seen in the forward scan at the potentials of 0.785 V (J_{f1}) and 1.209 V (J_{f2}), respectively and the third oxidation peak was observed during the backward scan at 0.486 V. The onset potential of a current rise at GC/PtNPs-chitosan, GC/PtNPs/FeNPs-chitosan, GC/PtNPs-CoNPs-chitosan, GC/PtNPs-CoNPs-FeNPs-chitosan electrodes was 0.24, 0.237, 0.224 and 0.2

V, respectively. The onset potential changes of as prepared electrodes were as follows:

PtNPs-CoNPs-FeNPs < PtNPs-CoNPs < PtNPs-FeNPs < PtNPs

The onset potential of EO on GC/PtNPs-CoNPs-FeNPs was less than other nanocatalysts showing that this catalyst has better catalytic activity toward ethanol electrooxidation. The anodic peak potential changes of EO at as-prepared electrodes were as follows:

E_{f1}: PtNPs-CoNPs-FeNPs = PtNPs < PtNPs-CoNPs < PtNPs-FeNPs

E_{f2}: PtNPs < PtNPs-CoNPs-FeNPs < PtNPs-CoNPs < PtNPs-FeNPs

The anodic peak potentials of EO at PtNPs-CoNPs-FeNPs nanocatalyst was less than PtNPs-CoNPs and PtNPs-FeNPs catalysts indicating that this catalyst has better catalytic activity toward ethanol electrooxidation. The first anodic current density (J_{f1}) of EO at GC/PtNPs-chitosan, GC/PtNPs-FeNPs-chitosan, GC/PtNPs-CoNPs-chitosan and GC/PtNPs-CoNPs-FeNPs-chitosan electrodes was 110.31, 146.73, 161.75 and 165.46 mA cm^{-2}, respectively and the second anodic current density (J_{f2}) was 183.71, 224.29, 245.99 and 275.60 mA cm^{-2}, respectively. Compared with the pure Pt catalyst, adding a certain amount of Fe and Co nanoparticles to the matrix of Pt nanocomposite can improve its catalytic activity for the EO reaction.

Our investigations showed that PtNPs-CoNPs-FeNPs nanocatalyst had higher catalytic activity toward ethanol electrooxidation due to the higher anodic current density, lower onset potential and lower anodic peak potentials. Also, EO reaction was investigated on GC/CoNPs-CH (4B (b)) and GC/FeNPs-CH (4B (c)) electrodes without any platinum. As seen in Fig. 4B (b) and 4B (c), these electrodes did not have any considerable activity for the EO reaction.

In order to investigate the EO reaction on Pt-based catalysts, knowing the mechanism of CO poisoning in the EO reaction seems to be important (Eqs. 3-12). The first reaction of ethanol with Pt nanoparticles is adsorption of ethanol on the Pt surface to give Pt(C_2H_5OH), which requires several free Pt binding sites. Then, dehydrogenation of ethanol begins on PtNPs surface. Pt-$(CO)_{ads}$ (Eq. 8), carbonaceous species such as acetaldehyde (Eqs. 5 and 6), acetic acid (Eq. 12) and methane (Eq. 9) are produced [30]. It is well known that the J_f peak involves the progress of these various steps and depends on the quantity of clean active sites available on PtNPs surface. Then, dissociation of water occurs on the pure Pt electrode and the produced OH groups remove the adsorbed CO from the Pt surface (Eqs. 10 and 11). The mechanism of EO on the platinum surface seems to be as follows:

$$Pt+CH_3\text{-}CH_2OH \rightarrow Pt\text{-}OCH_2\text{-}CH_3 + e + H^+ \quad (3)$$

$$Pt + CH_3\text{-}CH_2OH \rightarrow Pt\text{-}CHOH\text{-}CH_3 + e + H^+ \quad (4)$$

$$Pt\text{-}OCH_2\text{-}CH_3 \rightarrow Pt + CHO\text{-}CH_3 + e + H^+ \quad (5)$$

$$Pt\text{-}CHOH\text{-}CH_3 \rightarrow Pt + CHO\text{-}CH_3 + e + H^+ \quad (6)$$

$$Pt + CHO\text{-}CH_3 \rightarrow Pt\text{-}CO\text{-}CH_3 + e + H^+ \quad (7)$$

$$Pt\text{-}CO\text{-}CH_3 + Pt \rightarrow Pt\text{-}CO + Pt\text{-}CH_3 \quad (8)$$

$$Pt\text{-}CH_3 + Pt\text{-}H \rightarrow 2Pt + CH_4 \quad (9)$$

$$Pt + H_2O \rightarrow Pt\text{-}OH + e + H^+ \quad (10)$$

$$Pt\text{-}CO + Pt\text{-}OH \rightarrow 2Pt + CO_2 + e + H^+ \quad (11)$$

$$CHO\text{-}CH_3 + Pt\text{-}OH \rightarrow Pt + CH_3\text{-}COOH + e + H^+ \quad (12)$$

Electrochemical impedance spectroscopy (EIS) for ethanol electrooxidation

In the electrochemical impedance spectroscopy (EIS) investigations, the electrochemical performance of the working electrodes can be evaluated by Nyquist plot [31]. Generally, there is a semicircle part and a straight line in the Nyquist plot. The semicircle part in the high frequency region is due to a circuit containing a resistance element parallel to a capacitance element [32]. The straight line in the low frequency region corresponds to the Warbug impedance. Usually, the semicircle diameter equals the charge transfer resistance (R_{ct}). A smaller amount of the semicircle diameter and therefore a lower value of R_{ct} indicate the faster charge transfer reaction rate.

Fig. 5A illustrates the Nyquist plots of PtNPs-CH, PtNPs-FeNPs-CH, PtNPs-CoNPs-CH and PtNPs-CoNPs-FeNPs-CH nanocatalysts in the solution of

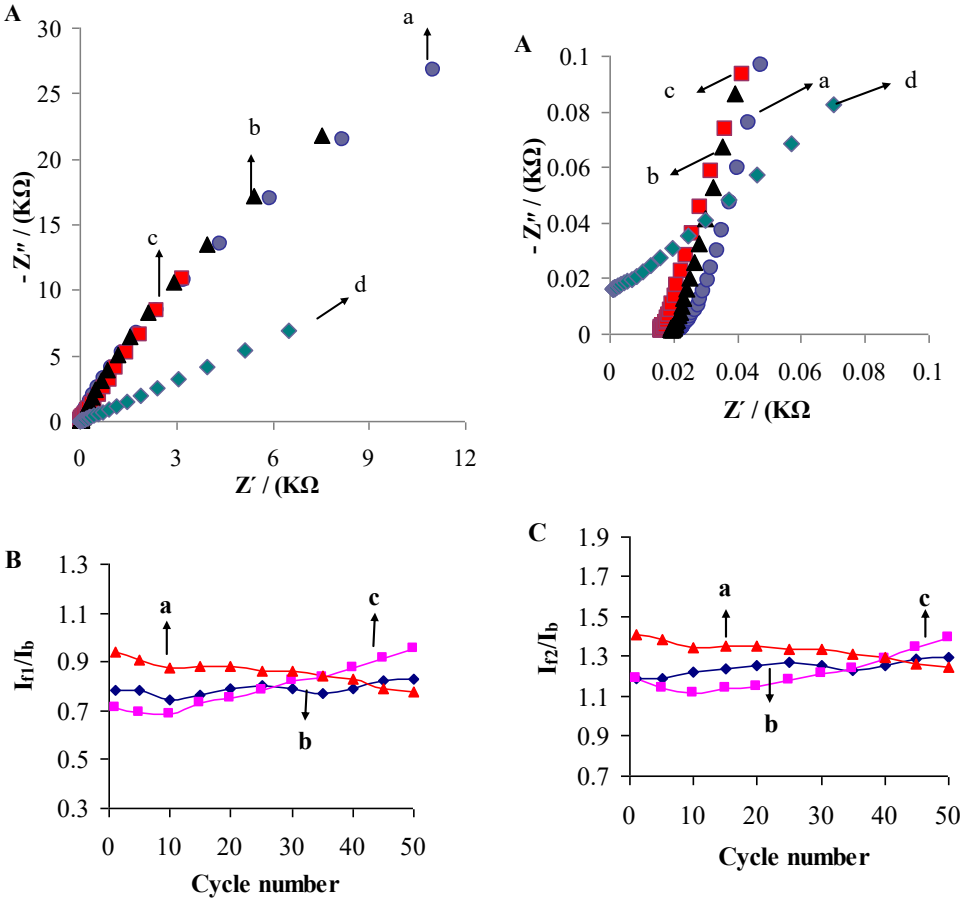

Fig. 5 A) Nyquist plots for a) PtNPs-CH, b) PtNPs-CoNPs-CH, c) PtNPs-FeNPs-CH, d) PtNPs-CoNPs-FeNPs-CH catalysts coated GC electrode in 0.5 M H_2SO_4, 1.07 M C2H5OH aqueous solution, B) the If1/Ib ratio and C) If2/Ib ratio of a) PtNPs-FeNPs, b) PtNPs-CoNPs and c) PtNPs-CoNPs-FeNPs electrodes as a function of the CV cycle number for EO reaction.

0.5 M H_2SO_4 and 1.07 M ethanol. EIS investigation was done at the open circuit potential (OCP). As seen in Fig 5A, all as prepared catalysts had a very small semicircle diameter in the high frequency region. For PtNPs-CoNPs-FeNPs-CH catalyst, the semicircle diameter was smaller than other catalysts. Therefore, the charge transfer process of EOR occurring on the PtNPs-CoNPs-FeNPs-CH catalyst is so faster than those on other nanocatalysts.

Durability test of the electrodes

In order to examine the poisoning effect of as-prepared electrodes during EO, catalytic activity of PtNPs-CoNPs-CH, PtNPs-FeNPs-CH and PtNPs-CoNPs-FeNPs-CH nanocomposites was investigated through cyclic voltammetry and 50 cycles repeatedly. The I_{f1}/I_b and I_{f2}/I_b ratios of as-prepared electrodes as a function of cycle number are shown in Fig. 5B and 5C, respectively. As observed for PtNPs-FeNPs-CH nanocomposite, I_{f1}/I_b and also I_{f2}/I_b ratios decreased during 50 cycles, indicating the poor anti-poisoning performance of this catalyst.

For PtNPs-CoNPs-CH, there was a gradual drop of I_{f1}/I_b ratio within the first 10 cycles, whereas it exhibited an increasing trend after 10 cycles, there was a little decrease from 25 to 35 cycles and again increased up to 50 cycles. Also, for PtNPs-CoNPs-CH, there was a gradual increase in the I_{f2}/I_b ratio during the first 25 cycles, it had a little decrease from 25 to 35 cycles and then increased up to 50 cycles. For PtNPs-CoNPs-CH catalyst, the maximum amounts of the I_{f1}/I_b and I_{f2}/I_b ratios were 0.83 and 1.29, respectively. For PtNPs-CoNPs-FeNPs-CH catalyst, the I_{f1}/I_b and I_{f2}/I_b ratios decreased during the first 10 cycles and it gradually increased up to 50 cycles. The maximum amounts of I_{f1}/I_b and I_{f2}/I_b ratios of PtNPs-CoNPs-FeNPs catalyst for EO reaction during the 50 cycles were 0.95 and 1.39,

respectively. PtNPs-CoNPs-FeNPs-CH catalyst had the highest I_{f1}/I_b and I_{f2}/I_b ratios after 50 cycles, indicating that this catalyst is capable of offering excellent antipoisoning effect toward EO.

Parameters affecting on electrooxidation of ethanol

Our investigations indicated that several factors such as ethanol concentration, Fe and Co amounts and scan rate were the main parameters influencing the performance of the proposed modified electrodes for ethanol electrooxidation.

Effect of ethanol concentration

Fig. 6 showed the effect of ethanol concentration on the anodic current density of EO on GC/PtNPs-

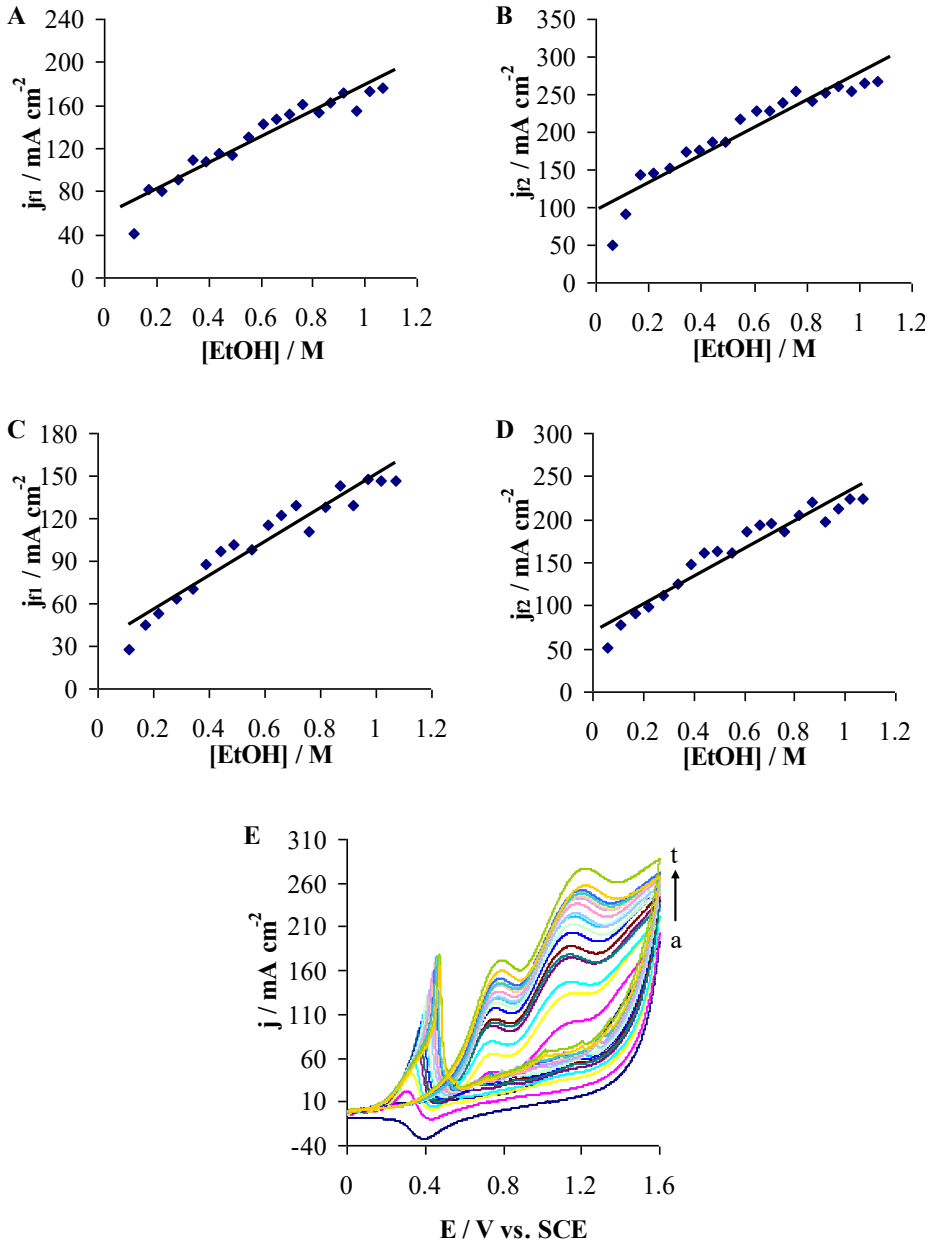

Fig. 6. Cyclic voltammograms for EO on A, B) PtNPs-CoNPs-CH ; C, D) PtNPs-FeNPs-CH and E) PtNPs-CoNPs-FeNPs-CH electrodes in 0.5 M H_2SO_4 in different concentration of ethanol: a) 0.06, b) 0.11, c) 0.17, d) 0.22, e) 0.28, f) 0.34, g) 0.39, h) 0.44, i) 0.49, j) 0.55, k) 0.61, l) 0.66, m) 0.71, n) 0.76, o) 0.82, p) 0.87, q) 0.92, r) 0.97, s) 1.02, t) 1.07 M.

CoNPs-CH (Fig. 6 A, B) and GC/PtNPs-FeNPs-CH (Fig. 6 C, D) electrodes. It was clearly observed that the anodic current density increases with increasing ethanol concentration and levels off at concentrations higher than 1.07 M. We assume this effect may be due to the saturation of active sites on the surface of the electrode. This also indicates further that the electrooxidation of ethanol at modified electrode is controlled by diffusion process. In accordance with this result, the optimum concentration of ethanol to obtain a higher current density may be considered as about 1.07 M.

At GC/PtNPs-CoNPs-CH electrode, when the ethanol concentration increases from 0.06 to 1.07 M, the E_{f1} shifts towards positive direction from 0.742 to 0.789 V (Fig. 6A) and E_{f2} shifts towards positive direction from 1.126 to 1.219 V (Fig. 6B). Increasing the ethanol concentration from 0.06 to 1.07 M at GC/PtNPs-FeNPs-CH electrode causes the shift in E_{f1} from 0.747 to 0.799 V (Fig. 6C) and E_{f2} shifts towards positive direction from 1.133 to 1.211 V (Fig. 6D). This may result from the following reason: The increase of the ethanol concentration will increase the poisoning rate of the Pt catalyst and cause a shift of the oxidative removal of the strongly adsorbed intermediates to a more positive potential [33].

The effect of ethanol concentration was also investigated at GC/PtNPs-CoNPs-FeNPs-CH electrode. Cyclic voltammograms were obtained in different concentrations of ethanol. The same behavior was observed (Fig. 6E). At GC/PtNPs-CoNPs-FeNPs-CH electrode, when the ethanol concentration increases from 0.06 to 1.07 M, the E_{f1} shifts towards positive direction from 0.729 to 0.79 V and E_{f2} shifts towards positive direction from 1.131 to 1.222 V.

Effect of Fe and Co nanoparticle amounts

In order to determine the effect of Co and Fe nanoparticle amounts, catalytic activity of PtNPs-FeNPs-CH and PtNPs-CoNPs-CH nanocatalysts toward ethanol electrooxidation was investigated through LSV under different concentrations of Fe and Co nanoparticles and constant amount of Pt nanoparticles (8mM) (Figs. 7A, 7B). Fig. 7A showed LSV curves of PtNPs-FeNPs-CH nanocomposite with 8mM of Pt nanoparticles and different concentrations 0.33, 0.99, 1.5 and 2.9 mM of Fe nanoparticles. As seen in Fig. 7A, the best catalytic activity was observed for PtNPs-FeNPs-CH with 8 mM Pt and 0.33 mM Fe nanoparticles. LSV curves of PtNPs-CoNPs-CH nanocatalysts with constant amount (8 mM) of Pt nanoparticles and different concentration (0.16, 0.33 and 0.49 mM) of Co nanoparticles were shown in Fig. 7B. Similarly, the best catalytic activity was observed for PtNPs-CoNPs-CH with 8 mM Pt and 0.33 mM Co nanoparticles.

Fig. 7. LSV curves of A) PtNPs-FeNPs-CH nanocomposite at 8mM PtNPs and a: 0.33, b: 0.99, c: 1.5, d: 2.9 mM of FeNPs and B) PtNPs-CoNPs-CH nanocomposites at 8 mM of PtNPs and a: 0.16, b: 0.33 and c: 0.49 mM of CoNPs.

Effect of scan rate

In order to investigate the effect of scan rate, the CV curves of PtNPs-CoNPs-CH, PtNPs-FeNPs-CH and PtNPs-CoNPs-FeNPs-CH were obtained at the scan rates of 30, 50, 70, 100, 150 and 200 mVs^{-1}. Based on the CV curves, the anodic peak current density amounts of ethanol oxidation vs.

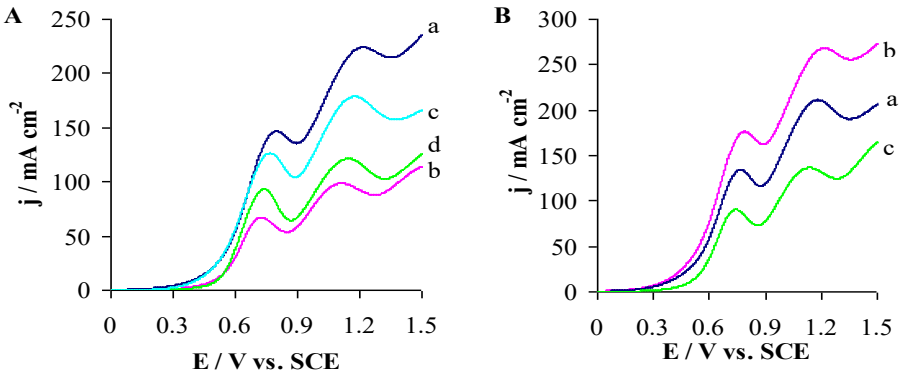

Fig. 7. LSV curves of A) PtNPs-FeNPs-CH nanocomposite at 8mM PtNPs and a: 0.33, b: 0.99, c: 1.5, d: 2.9 mM of FeNPs and B) PtNPs-CoNPs-CH nanocomposites at 8 mM of PtNPs and a: 0.16, b: 0.33 and c: 0.49 mM of CoNPs.

the square root of the sweeping rate and the peak potential vs. ln υ have been displayed (Fig. 8). The experiments have been done in 1.07 M ethanol and 0.5 M H_2SO_4 medium at different scan rates.

As seen in Fig. 8, by increasing the applied sweeping rate, the anodic peak current density of ethanol oxidation has been increased. The linear relationship (R^2 = 0.92 - 0.96) between the square root of the scan rate and the first peak current density (j_{f1}) and also a linear relationship (R^2 = 0.98 - 0.99) between the square root of the scan rate and the second peak current density (j_{f2}) demonstrates that EO process is controlled with diffusion of ethanol from the bulk solution to the electrode surface [34, 35].

As observed in Fig. 8, the peak potential of ethanol oxidation (E_{f1}) and also (E_{f2}) amplified with increasing the scan rate, and a linear relationship (R^2 = 0.94 - 0.98) between E_{f1} and ln (υ) and also a linear relationship (R^2=0.93 - 0.99) between E_{f2} and ln (υ) has been obtained. This shows that ethanol oxidation is an irreversible charge transfer process [36, 37].

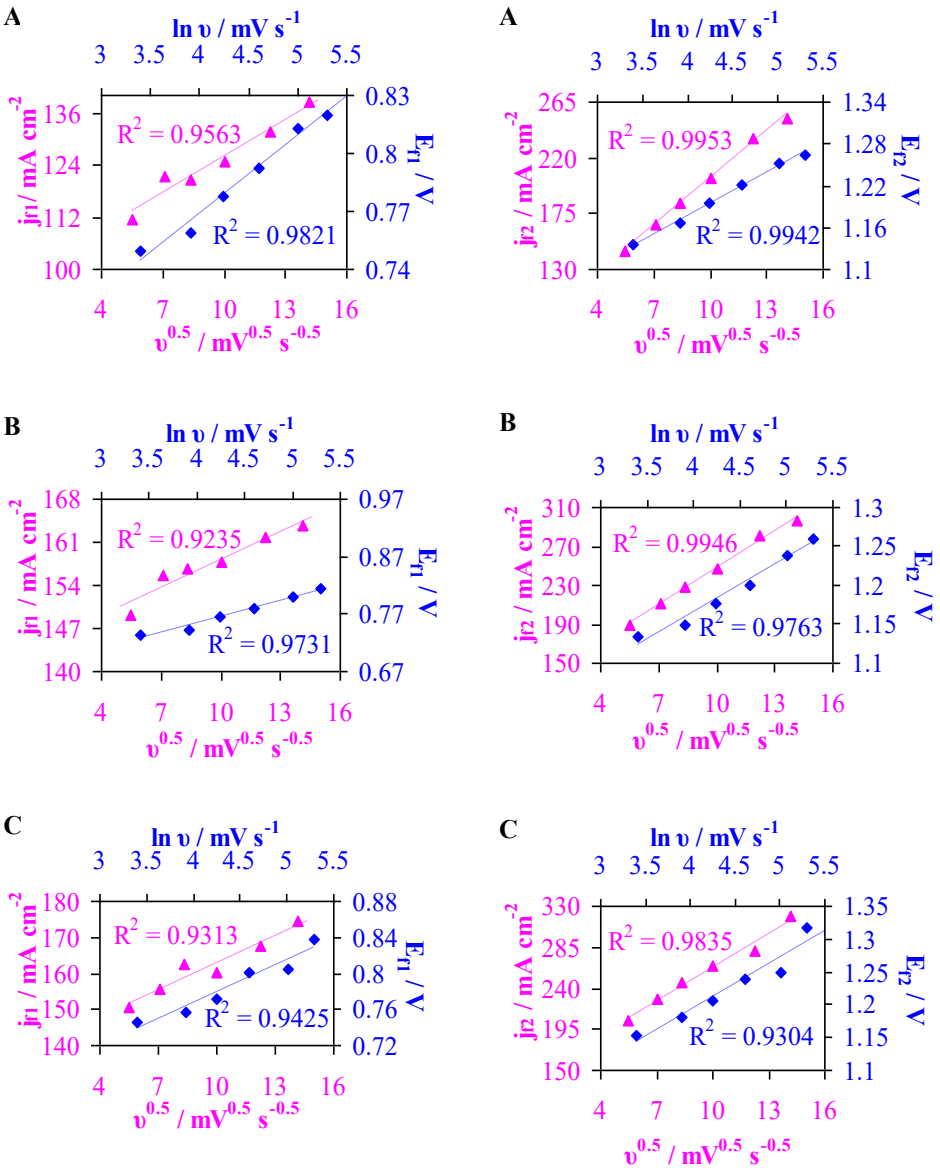

Fig. 8. Anodic current density (jf1 and jf2) vs. square root of scan rate ($υ^{0.5}$) and irreversibility plot of peak potential (Ef1 and Ef2) vs. ln υ for A) PtNPs-FeNPs-CH, B) PtNPs-CoNPs-CH, C) PtNPs-CoNPs-FeNPs-CH electrodes in 1.07 M ethanol and 0.5 M H_2SO_4 at the scan rates of 30, 50, 70, 100, 150 and 200 mV s^{-1}.

Effect of temperature

The effect of temperature on the electrocatalytic activity of PtNPs-CoNPs-CH, PtNPs-FeNPs-CH and PtNPs-CoNPs-FeNPs-CH nanocatalysts toward ethanol oxidation was investigated through CV curves obtained in different temperatures ranging from 20 to 45˚C (Fig. 9). As seen in Fig. 9, the anodic current density was increased with increasing of the temperature. In this way, the mass transport is an important factor for higher activity. As observed for PtNPs-FeNPs-CH nanocatalyst in Fig. 9A, when the temperature changed from 20 to 45˚C, j_{f1} increased from 140.43 to 234.35 mA cm^{-2} and j_{f2} increased from 223.59 to 329.91 $mAcm^{-2}$. For PtNPs-CoNPs-CH nanocatalyst, when the temperature increased from 20 to 45 ˚C, j_{f1} increased from 169.46 to 232.36 mA cm^{-2} and j_{f2} increased from 266.88 to 349.23 mA cm^{-2} as shown in Fig. 9B.

The effect of temperature on the catalytic activity of PtNPs-CoNPs-FeNPs-CH for ethanol

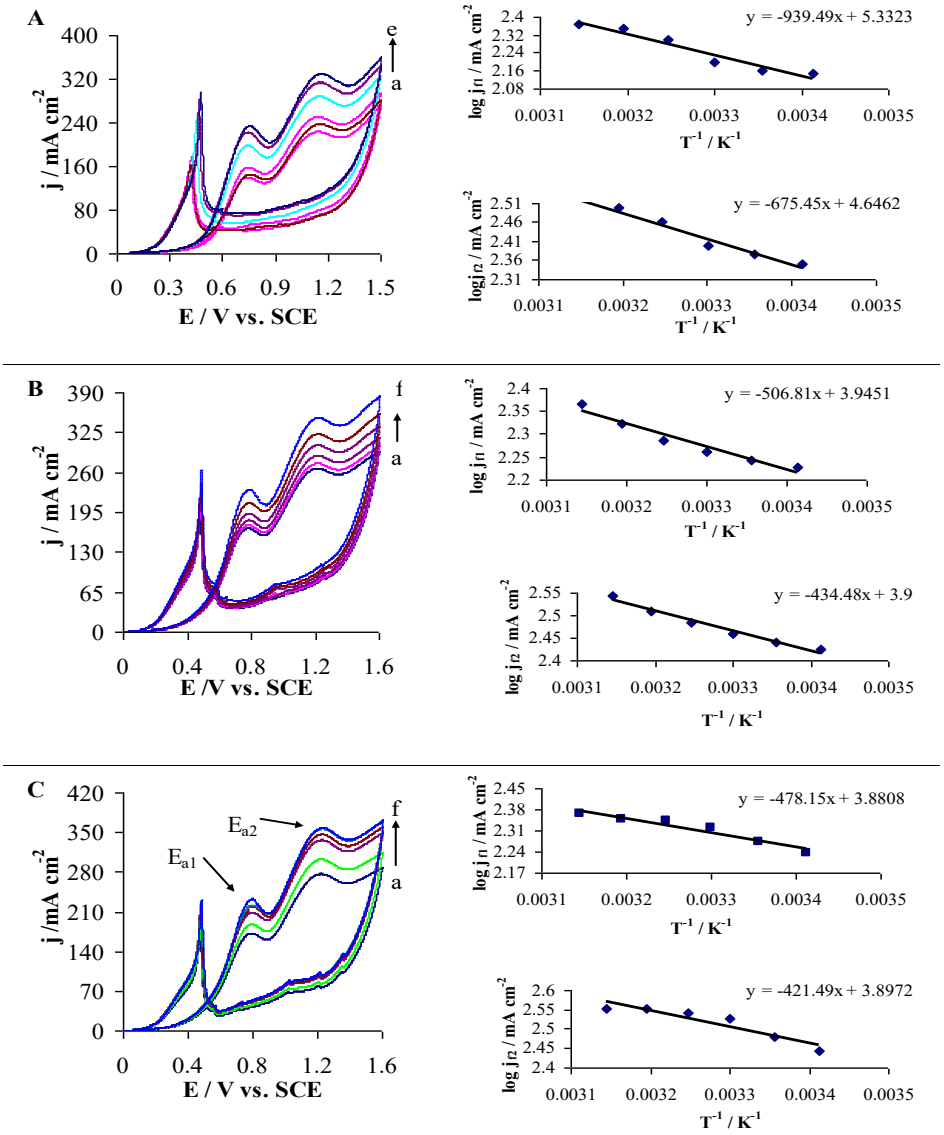

Fig. 9. Cyclic voltammograms and Arrhenius plots of the logarithm of exchange current density (log jf) versus the reciprocal of temperature (T-1) of A) PtNPs-FeNPs-CH, B) PtNPs-CoNPs-CH and C) PtNPs-CoNPs-FeNPs-CH nanocatalysts in different temperatures of a) 20, b) 25, c) 30, d) 35, e) 40 and f) 45 ˚C

electrooxidation was shown in Fig. 9C. As seen in Fig. 9C, when the temperature increased from 20 to 45 ˚C, j_{f1} increased from 172.21 to 232.96 mA cm^{-2} and j_{f2} increased from 277.24 to 358.24 mA cm^{-2}. As seen for all the catalysts, the ethanol oxidation activity was enhanced as the temperature increased. At the same ethanol concentration, the higher current density indicated that the nano sized catalysts possess more available active sites of three metals to participate in the electrochemical reaction.

Activation energies were calculated by investigating the EO reaction at different temperatures between 20 and 45 ˚C on GC/PtNPs-FeNPs-CH, GC/PtNPs-CoNPs-CH and GC/PtNPs-CoNPs-FeNPs-CH electrodes. Arrhenius plots of logarithm of exchange current density (log j_p) versus the reciprocal of temperature (T^{-1}) were shown in Fig. 9. Activation energies were calculated from the slope of the Arrhenius plots for certain potential values using Eq. (13):

$$\partial \ln j_p / \partial(1/T) = E_a/R \quad (13)$$

The apparent activation energy of the first anodic peak of ethanol electrooxidation (E_{a1}) at PtNPs-FeNPs-CH, PtNPs-CoNPs-CH and PtNPs-CoNPs-FeNPs-CH electrodes was 7.81, 4.21 and 3.97 kJ mol^{-1}, respectively. The activation energy of the second anodic peak of ethanol oxidation (E_{a2}) at PtNPs-FeNPs-CH, PtNPs-CoNPs-CH and PtNPs-CoNPs-FeNPs-CH electrodes was 5.62, 3.61 and 3.50 kJ mol^{-1}, respectively. Lower activation energy of ethanol electrooxidation at PtNPs-CoNPs-FeNPs-CH electrode indicated that this electrode has better catalytic activity than other prepared catalysts toward ethanol electrooxidation.

Amperometric i-t curve measurements

The activities of the prepared catalysts toward EO measured by steady state current densities at a constant potential were used for comparing the catalytic performance of all as-prepared catalysts. Amperometric i-t curve measurements were carried out at potential value 1 V in 1.07 M ethanol and 0.5 M H_2SO_4 (Fig. 10). Fig. 10A showed the amperometric i-t curves of PtNPs-CH, PtNPs-FeNPs-CH, PtNPs-CoNPs-CH and PtNPs-CoNPs-FeNPs-CH nanocomposites with the concentrations of Pt (8 mM), Fe and Co nanoparticles (0.33 mM).

As seen in Fig. 10A, the initial high current densities correspond to the double-layer charging [38]. All potentiostatic currents decreased rapidly in the initial stage. After a period of 80 s, the current decay became gradual and then remained stable. After 100 s, the current density of all the catalysts became almost constant. The steady-state part of the curve indicated that the stable current of PtNPs-CoNPs-FeNPs-CH electrode was higher than in the other three catalysts. This result revealed that PtNPs-CoNPs-FeNPs-CH catalyst has the highest electrocatalytic activity toward ethanol electrooxidation and the highest stability. Thus, PtNPs-CoNPs-FeNPs-CH catalyst seems to be a promising candidate for the direct ethanol fuel cell applications.

Electrocatalytic activity of GC/PtNPs-CoNPs-FeNPs-CH electrode toward ethanol electrooxidation was also investigated with different concentration of Fe and Co nanoparticles. In order to investigate the effect of FeNPs concentration, chronoamperometry curves were obtained in the constant amount of Co nanoparticles (0.33 mM) and different concentrations (0.33, 0.99, 2.9 mM) of Fe nanoparticles (Fig. 10B).

To determine the effect of Co concentration on the catalytic activity of GC/PtNPs-CoNPs-FeNPs-CH electrode for ethanol electrooxidation, constant amount of Fe nanoparticles (0.33 mM) and different concentration of CoNPs (0.16, 0.33, 0.49 mM) were used (Fig. 10C). The best result was observed for PtNPs-CoNPs-FeNPs-CH nanocomposite with Pt 8 mM, Co 0.33 mM and Fe 0.33 mM composition.

CONCLUSIONS

In this work, Pt-M-chitosan (M = Co, Fe) nanocomposites dispersed in chitosan polymer were successfully synthesized and characterized. The GC/PtNPs-CoNPs-CH, GC/PtNPs-FeNPs-CH and GC/PtNPs-CoNPs-FeNPs-CH electrodes were prepared as active electrocatalysts for electrooxidation of ethanol. Good dispersion of the metal nanoparticles shown in the TEM images revealed that chitosan is a good support for preparation of the metal nanoparticles. Our results showed that, incorporation of Co and Fe nanoparticles into the Pt catalyst can improve the electrode performance for ethanol electrooxidation. The activity of PtNPs-CoNPs-FeNPs-CH for ethanol electrooxidation in acid medium was higher than that of PtNPs-CoNPs-CH, PtNPs-FeNPs-CH and also much higher

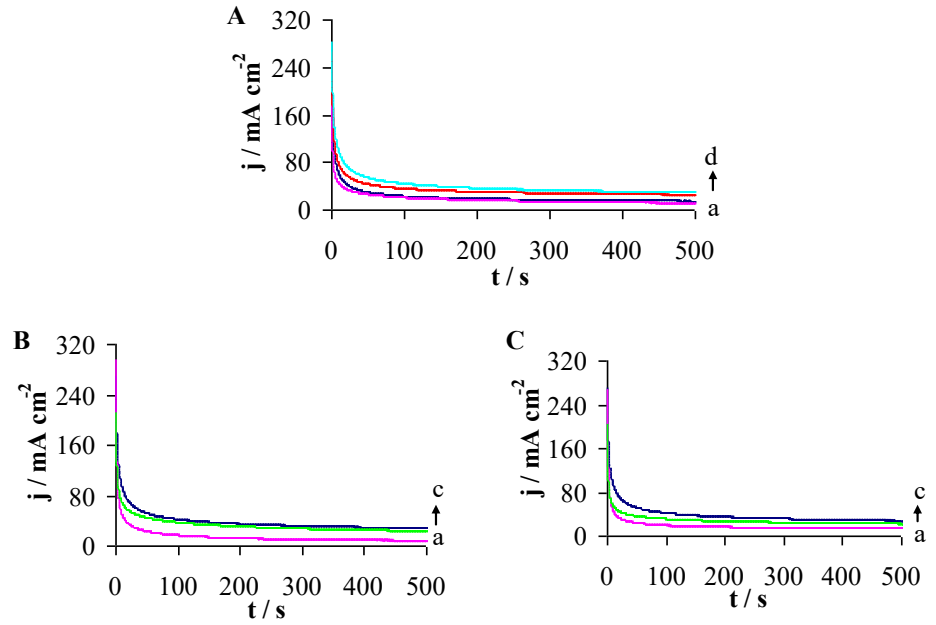

Fig. 10. Chronoamperometry for EO at A) all prepared catalysts, B) GC/PtNPs-CoNPs-FeNPs-CH electrocatalyst with 0.33 mM of CoNPs and different concentrations of FeNPs: a) 0.99, b) 2.9, c) 0.33 mM and C) GC/PtNPs-CoNPs-FeNPs-CH electrocatalyst with 0.33 mM of FeNPs and different concentrations of CoNPs: a) 0.16, b) 0.49, c) 0.33 mM in 1.07 M ethanol and 0.5 M H_2SO_4.

than that of PtNPs-CH catalyst due to its higher current density, lower anodic peak potential, higher electrochemically active surface area and better antipoisoning effect toward EO obtained after 50 cycles. This result was confirmed with comparing of the activation energy, the amperometric i-t curves, the CO stripping and the EIS investigations of the prepared catalysts. The CO stripping investigations showed that PtNPs-CoNPs-FeNPs-CH catalyst had higher CO tolerance than other prepared catalysts. CO produced from ethanol dissociation can be easily oxidized to CO_2 on this catalyst. In this case the CO poisoning of PtNPs-CoNPs-FeNPs-CH catalyst was lower than other as-prepared catalysts. All the investigations revealed that PtNPs-CoNPs-FeNPs-CH catalyst had the best catalytic activity toward ethanol electrooxidation.

ACKNOWLEDGMENT

We thank Esfarayen University of Technology for financial support.

CONFLICT OF INTEREST

The authors declare that there are no conflicts of interest regarding the publication of this manuscript.

REFERENCES

1. Soliman AB, Abdel-Samad HS, Abdel Rehim SS, Ahmed MA, Hassan HH. High Performance Nano-Ni/Graphite Electrode for Electro-oxidation in Direct Alkaline Ethanol Fuel Cells. J. Power Sources, 2016; 325: 653-663.
2. Antoniassi RM, Otubo L, Vaz JM, Oliveira Neto A, Spinacé EV. Synthesis of Pt Nanoparticles with Preferential (100) Orientation Directly on the Carbon Support for Direct Ethanol Fuel Cell. J. Catal., 2016; 342: 67-74.
3. Mao H, Huang T, Yu A. Surface Noble Metal Modified PdM/C (M=Ru, Pt, Au) as Anode Catalysts for Direct Ethanol Fuel Cells. J. Alloy. Compd., 2016; 676: 390-396.
4. Liu X, Duan J, Chen H, Zhang Y, Zhang X. A Carbon Riveted Pt/Graphene Catalyst with High Stability for Direct Methanol Fuel Cell. Microelectron. Eng., 2013; 110: 354-357.
5. Higuchi E, Takase T, Chiku M, Inoue H. Preparation of Ternary Pt/Rh/SnO2 Anode Catalysts for Use in Direct Ethanol Fuel Cells and Their Electrocatalytic Activity for Ethanol Oxidation Reaction. J. Power Sources, 2014; 263: 280-287.
6. Kéranguéven G, Berná A, Siber E, Feliu JM, Léger JM. Dimethoxymethane Electrooxidation on Low Index Planes of Platinum Single Crystal in Acid Media. Electrochim. Acta, 2008; 54 (2): 394-402.
7. Shin JH, Yoon JH, Lee SH, Park TH. Hydrogen Production from Formic Acid in pH-Stat Fed-Batch Operation for Direct Supply to Fuel Cell. Bioresour. Technol., 2010; 101 (1): S53- S58.
8. Faro ML, Rosa DL, Nicotera I, Antonucci V, Salvatore Aricò

A. Electrochemical Investigation of a Propane-Fed Solid Oxide Fuel Cell Based on a Composite Ni–Perovskite Anode Catalyst. Appl. Catal. B Environ., 2009; 89 (1-2): 49-57.

9. Ureta-Zanartu MS, Alarcon A, Munoz G, Gutiérrez C. Electrooxidation of Methanol and Ethylene Glycol on Gold and on Gold Modified with an Electrodeposited PolyNiTSPc Film. Electrochim. Acta, 2007; 52 (28): 7857-7864.
10. Wu B, Cui R, Gao Y, Jiang Z. Ethanol Electrocatalytic Oxidation on Highly Dispersed Pt-TiO_2/C Catalysts. Russ. J. Electrochem., 2009; 45 (7): 731-735.
11. Lamy C, Belgsir EM, Léger JM. Electrocatalytic Oxidation of Aliphatic Alcohols: Application to the Direct Alcohol Fuel Cell (DAFC). J. Appl. Electrochem., 2001; 31 (7): 799-809.
12. Zhou W, Zhou Z, Song S, Li W, Sun G, Tsiakaras P, Xin Q. Pt Based Anode Catalysts for Direct Ethanol Fuel Cells. Appl. Catal. B: Environ., 2003; 46 (2): 273-285.
13. Rizo R, Sebastián D, Jesús Lázaro M, Pastor E. On the Design of Pt-Sn Efficient Catalyst for Carbon Monoxide and Ethanol Oxidation in Acid and Alkaline Media. Appl. Catal. B, 2017; 200: 246-254.
14. Ammam M, Bradley Easton E. Quaternary PtMnCuX/C (X=Fe, Co, Ni, and Sn) and $PtMnMo_x$/C (X=Fe, Co, Ni, Cu and Sn) Alloys Catalysts: Synthesis, Characterization and Activity towards Ethanol Electrooxidation. J. Power Sources, 2012; 215: 188-198.
15. Ekrami-Kakhki MS, Khorasani-Motlagh M, Noroozifar M. Platinum Nanoparticles Self-Assembled onto Chitosan Membrane as Anode for Direct Methanol Fuel Cell. J. Appl. Electrochem., 2011; 41 (5): 527-534.
16. Tang Z, Geng D, Lu G. A Simple Solution-Phase Reduction Method for the Synthesis of Shape-Controlled Platinum Nanoparticles. Mater. Lett., 2005; 59 (12): 1567-1570.
17. Su YK, Shen CM, Yang TZ, Yang HT, Gao HJ, Li HL. The Dependence of Co Nanoparticle Sizes on the Ratio of Surfactants and the Influence of Different Crystal Sizes on Magnetic Properties. Appl. Phys. A, 2005; 81 (3): 569-572.
18. Mazumdar H, Haloi N. A Study on Biosynthesis of Iron Nanoparticles by Pleurotus sp. J. Microbiol. Biotech. Res., 2011; 1 (3): 39-49.
19. Venkateswara RC, Singh SK, Viswanathan B. Electrochemical Performance of Nano-SiC Prepared in Thermal Plasma. Indian J. Chem., 2008; 47A (11): 1619-1625.
20. Wang H, Wang R, Li H, Wang Q, Lei Z. Facile Synthesis of Carbon-Supported Pseudo-Core@Shell PdCu@Pt Nanoparticles for Direct Methanol Fuel Cells. Int. J. Hydrogen Energy, 2011; 36 (1): 839-848.
21. Noroozifar M, Khorasani-Motlagh M, Ekrami-Kakhki MS. Enhanced Electrocatalytic Properties of Pt–Chitosan Nanocomposite for Direct Methanol Fuel Cell by $LaFeO_3$ and Carbon Nanotube. J. Power Sources, 2014; 248: 130-139.
22. Liu YT, Yuan QB, Duan DH, Zhang ZL, Hao XG, Wei GQ, Liu SB. Electrochemical Activity and Stability of Core–Shell Fe2O3/Pt Nanoparticles for Methanol Oxidation. J. Power Sources, 2013; 243: 622-629.
23. Sivakumar P, Tricoli V. Novel Pt–Ru Nanoparticles Formed by Vapour Deposition as Efficient Electrocatalyst for Methanol Oxidation: Part II. Electrocatalytic Activity. Electrochim. Acta, 2006; 51 (7): 1235-1243.
24. Morimoto Y, Yeager EB. CO Oxidation on Smooth and High Area Pt, Pt-Ru and Pt-Sn Electrodes. J. Electroanal. Chem., 1998; 441 (1-2): 77-81.
25. Massong H, Wang H, Samjeske G, Baltruschat H. The Co-Catalytic Effect of Sn, Ru and Mo Decorating Steps of Pt(111) Vicinal Electrode Surfaces on the Oxidation of CO. Electrochim. Acta, 2001; 46 (5): 701-707.
26. Wang K, Gasteiger HA, Markovic NM, Ross Jr PN. On the Reaction Pathway for Methanol and Carbon Monoxide Electrooxidation on Pt-Sn Alloy versus Pt-Ru Alloy Surfaces. Electrochim. Acta, 1996; 41 (16): 2587-2593.
27. Kulesza P, Matczak M, Wolkiewicz A, Grzybowska B, Galkowski M, Malik MA, Wieckowski A. Electrocatalytic Properties of Conducting Polymer Based Composite Film Containing Dispersed Platinum Microparticles towards Oxidation of Methanol. Electrochim. Acta, 1999; 44 (12): 2131- 2137.
28. Fujiwara N, Friedrich KA, Stimming U. Ethanol Oxidation on PtRu Electrodes Studied by Differential Electrochemical Mass Spectrometry. J. Electroanal. Chem., 1999; 472 (2): 120-125.
29. Saleh FS, Easton EB. Assessment of the Ethanol Oxidation Activity and Durability of Pt Catalysts with or without a Carbon Support using Electrochemical Impedance Spectroscopy. J. Power Sources, 2014; 246: 392-401.
30. Vigier F, Coutanceau C, Hahn F, Belgsir EM, Lamy C. On the Mechanism of Ethanol Electro-oxidation on Pt and PtSn Catalysts: Electrochemical and in Situ IR Reflectance Spectroscopy Studies. J. Electroanal. Chem., 2004; 563 (1): 81-89.
31. Ding K, Jia Z, Wang Q, He X, Tian N, Tong R, Wang X. Electrochemical Behavior of the Self-Assembled Membrane Formed by Calmodulin (CaM) on a Au Substrate. J. Electroanal. Chem., 2001; 513 (1): 67-71.
32. Ding K, Jia H, Wei S, Guo Z. Electrocatalysis of Sandwich-Structured Pd/Polypyrrole/Pd Composites toward Formic Acid Oxidation. Industr. Eng. Chem. Res., 2011; 50 (11): 7077-7082.
33. He Z, Chen J, Liu D, Zhou H, Kuang Y. Electrodeposition of Pt–Ru Nanoparticles on Carbon Nanotubes and their Electrocatalytic Properties for Methanol Electrooxidation. Diam. Relat. Mater., 2004; 13 (10): 1764-1770.
34. Khaleghian-Moghadam R, Noroozifar M, Khorasani Motlagh M, Ekrami-Kakhki MS. Electrochemical Activities of Platinum-Decorated Multi-wall Carbon Nanotube/Chitosan Composites for the Oxidations of Alcohols. J. Solid State

Electrochem., 2013; 17 (3): 643-654.

35. Zhao Y, Wang R, Han Z, Li C, Wang Y, Chi B, Li J, Wang X. Electrooxidation of Methanol and Ethanol in Acidic Medium Using a Platinum Electrode Modified with Lanthanum-Doped Tantalum Oxide Film. Electrochim. Acta, 2015; 151: 544-551.
36. Guo DJ, Li HL. Electrocatalytic Oxidation of Methanol on Pt Modified Single-Walled Carbon Nanotubes. J. Power Sources, 2006; 160 (1): 44- 49.
37. Noroozifar M, Khorasani-Motlagh M, Khaleghian-Moghadam R, Ekrami-Kakhki MS, Shahraki M. Incorporation Effect of Nanosized Perovskite $LaFe_{0.7}Co_{0.3}O_3$ on the Electrochemical Activity of Pt Nanoparticles-Multi Walled Carbon Nanotube Composite toward Methanol Oxidation. J. Solid State Chem., 2013; 201: 41-47.
38. Wang ZB, Yin GP, Zhang J, Sun YC, Shi PF. Investigation of Ethanol Electrooxidation on a Pt–Ru–Ni/C Catalyst for a Direct Ethanol Fuel Cell. J. Power Sources, 2006; 160 (1): 37-43.